A near wake model for deformable trailing edge flaps implemented the in multi body aero-servo-elastic code HAWC2

Andersen, Peter Bjørn; Aagaard Madsen, Helge; Gaunaa, Mac

Published in:
EWEC 2010 Proceedings online

Publication date:
2010

Document Version
Publisher's PDF, also known as Version of record

ABSTRACT:

The presented paper contains an extended version of the near wake model for trailing vorticity originally proposed by Beddoes [4] and implemented in the work of Madsen et al. [9]. The near wake model has been further developed to include a tuning method which provides a better fit to the Biot-Savart equation compared to the one suggested by Beddoes in 1987. The planar arc extension from Wang and Coton has been implemented which makes the vortex filament shift away from the rotor plane, adding a tangential induction component to the near wake model. A sub-time domain modal is formulated to speedup calculation time. The far wake is taken into account by a series of thrust and tip-speed lookups. The present model is compared to the general unsteady vortex particle model developed at code was developed at the national technical university of Athens, where ten minute series of the normal force at 75% radius is compared using the rainflow counting technique. Using a 1000 meter long blade the calculated induction is compared to the analytical expression for an elliptic circulation. By mounting a trailing edge flap to a section of the blade it is possible to see the radial interaction between the sections which the near wake model offers as opposed to the traditional blade element momentum method.

KEY WORDS:

Near Wake, Far Wake, Induction, Indicial Function, Blade Element Momentum, Vortex, Trailed Vorticity, Shed Vorticity

INTRODUCTION:

The Blade Element Momentum (BEM) model is often used in aero-elastic codes for predicting the behavior of wind turbines. The computational speed and CPU requirement for a BEM computation makes it a prudent choice when unsteady loads have to be determent. However, the traditional BEM code depends heavily on input from airfoil data and three dimensional flow effects are not readily considered due to the steam tube strips assumption which founds the derivation of the axial induction. Another fundamental shortcoming of the BEM code is that it is a steady state model, on wind turbine rotors the loading is highly dynamic due to turbulence, actuators and various eigen motions. Various computational fluid dynamics (CFD) codes offers a detailed three dimensional flow, but is considered slow for longer unsteady load computations. This paper presents another approach for determining the unsteady wake based on the lifting line and vortex formulation which have shown to be a good balance between computational speed and accuracy. The complete vortex system behind a rotating blade in an unsteady environment consists of the trailed vorticity due to radial variation in the bound circulation along the blade and the shed vorticity from the time variation of the bound circulation. By considering only the trailed vortex system of one quarter of a revolution, it is possible to approximate the single blade near wake contribution to the downwash by exponential functions. The original proposed two term indicial approximation by Beddoes [4] of the normalized Biot-Savart circular vortex arc equation have been replaced by a simplex optimization engine which guaranties a better fit to this equation using more indicial terms which can be seen in Figure 1. Besides the near wake contribution to the induction it is also necessary to consider the contribution from the other blades and the far wake in general. This is done by

scaling the rotor loading down so total downwash becomes correct. The total loading of the rotor, to be scaled, is given by the dynamic inflow model. An effort is made in the new model to ensure the far wake influence is included by scaling the total rotor loading and tip-speed using a surface fit. In addition to trailed vorticity, the wake system also comprises a shed vorticity part given by the dynamic stall model for the deformable trailing edge flaps proposed by Andersen et al. [2]. High frequency changes in loads are captured by the dynamic stall model and the near wake model deals with the mid ranges, whereas, the far wake model accounts for the induction from the slow changes in loading.

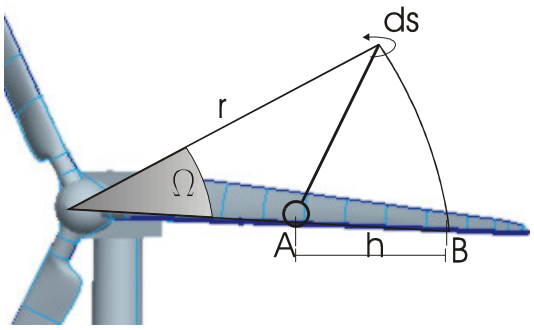

Figure 1; model geometry for the near wake model, azimuth angle is *Ω*, distance between two points *A*,*B* on blade is *h* and the length *ds* of a trailed vortex element at radius *r* contributing to the induction at point A.

The present model offers a better approximation to the normalized Biot-Savart equation, as the approximation to the decay rates have been improved the effect of this is investigated in a series of pitch step changes, and the considerable variation in induction response time along the blade is illustrated and compared to previous results by Beddoes. The full wake model comprised by the near and far wake trailed vorticity and the shed vorticity is implemented in HAWC2 [7]. A two meter Deformable Trailing Edge Flap (DTEF) will be added to the blade and actuated causing a response in the full dynamic wake, the axial induction will be plotted in a three dimensions illustrating the strong redial dependency which now is captured by the model. In prior investigations by Andersen et al. [1] the radial dependency of the axial induction provided by the near wake model was not considered when the potential of smart materials to wind turbine blades was investigated. A few runs will compare the effect of applying the near wake model to the 5MW reference turbine used in the Upwind project [13]. Different methods of modeling dynamic inflow in aero-elastic codes are described in reference [11] and [10].

NEAR WAKE MODEL:

The near wake geometry illustrated in Figure 1 does not comprise shed vorticity and far wake the trailed vorticity, but it follows Beddoes [4] formulation which takes a point *A* on the rotating blade the induced vorticity *dw* from a vortex element of length *ds* and strength *Γ* at radius *r* is

$$dw = \frac{\Gamma ds}{4\pi r^2} \frac{1 - \left(1 - \frac{h}{r}\right) cos(\Omega)}{\left[1 + \left(1 - \frac{h}{r}\right)^2 - 2\left(1 - \frac{h}{r}\right) \cos(\Omega)\right]^{3/2}} \quad (1)$$

normalized with the initial value of the downwash dw_0 the equation becomes

$$\frac{dw}{dw_0} = \frac{|h|\frac{h}{r^2}\left(1-\left(1-\frac{h}{r}\right)cos(\Omega)\right)}{\left[1+\left(1-\frac{h}{r}\right)^2-2\left(1-\frac{h}{r}\right)\cos\left(\Omega\right)\right]^{3/2}} \tag{2}$$

, where the initial downwash dw_0 is

$$dw_0 = \frac{\Gamma ds}{4\pi h|h|} \tag{3}$$

, where the steady and unsteady circulation Γ_{st} and Γ is based on chord length c, relative velocity V_r and lift coefficient C_L and found using Youkowsky's law;

$$\Gamma_{st} = \frac{1}{2}V_r c C_L \tag{4}$$

Similar to the time lag between geometric and effective incidence in a dynamic stall model such as the Beddoes-Leishmann [2] the unsteady circulation can lag the steady circulation using

$$\Gamma = \Gamma_{st}[1-\epsilon_1-\epsilon_2]\gamma_1+\gamma_2 \tag{5}$$

where the circulation state variables are given by

$$\frac{\partial \gamma_n}{\partial t}+\varepsilon_n\gamma_n = \varepsilon_n\epsilon_n\Gamma_{st} \tag{6}$$

The initial function technique was also initially suggested by Beddoes to approximate Equation (2) by a series of exponential functions

$$\frac{dw}{dw_0} = \sum_{k=1}^{n} c_k e^{b_k\frac{\Omega}{\Phi}} \tag{7}$$

Equation (7) represents the decay of influence from the trailed circulation for the vortex element as a function of the circular path. The contribution at time step "*i*" to the downwash from one circular arc written up in numerical form is;

$$w(i) = \sum_{k=1}^{n} Z_k(i) \tag{8}$$

$$Z_k(i) = Z_k(i-1)e^{b_k\frac{\Delta\Omega}{\Phi}} + c_k D_w e^{b_k\frac{\Delta\Omega}{2\Phi}} \tag{9}$$

$$\Phi = \frac{\pi}{4}\left|\left(1+\frac{h}{2r}\right)ln\left(1-\frac{h}{r}\right)\right| \tag{10}$$

, where the axial downwash contribution D_w from the currently generated vortex element is given as

$$D_w = \frac{\Gamma\left|\Delta\Omega\frac{r}{h}\right|cos(\varphi)}{4\pi h\sqrt{1+\left(\Delta\Omega\frac{r}{h}\right)^2}} \tag{11}$$

The total axial downwash at point A equals the sum of all the circular vortex parts originating from the blades. The original model is based on the assumption that the trailed vorticity is to be found in the rotor plane, which is a reasonable assumption for the outer part of the blade where the local tip speed ratio is high, however, for the inner part of the blade the local tip speed ratio is low and the vorticity sheet can be tilted as much as 45 degrees relative to the rotor plane. Wang and Coton's [16] planar arc extension has been implemented where a tilting angle φ is introduced as

$$tan(\varphi) = \frac{V_\infty cos(\gamma) + w_B}{\omega r + V_\infty sin(\gamma)sin(\psi) + u_B} \tag{12}$$

, where the V_∞ is the free stream velocity, ω the angular velocity, ψ the blade azimuthal angle and γ is the angle between the direction normal to the rotor plane and the free stream velocity shown in Figure 2. Finally w_B and u_B are the axial and tangential velocities at point B.

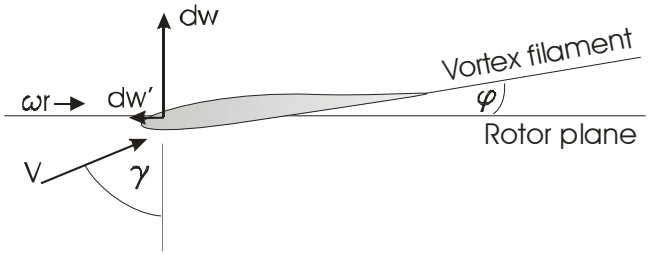

Figure 2; circular arc line vortex with cross-plane convection

Due to the cross-plane convection given by Equation (12), contributions to the tangential induction can be found by using equations identical to the axial induction.

$$w'(i) = \sum_{k=1}^{n} Z'_k(i) \tag{13}$$

$$Z'_k(i) = Z'_k(i-1)e^{b_k\frac{\Delta\Omega}{\Phi}} + c_k D'_w e^{b_k\frac{\Delta\Omega}{2\Phi}} \tag{14}$$

$$D'_w = \frac{\Gamma\left|\Delta\Omega\frac{r}{h}\right| sin(\varphi)}{4\pi h\sqrt{1+\left(\Delta\Omega\frac{r}{h}\right)^2}} \tag{15}$$

, D'_w represents the tangential downwash contribution from the currently generated vortex element and w' the total tangential induction at a given radial position on the blade.

Another extension to the work of Beddoes [4] and Wang and Coton [16] is presented in this paper. In order to calculate the total downwash a given point on the blade only "n" numbers have to be stored. Beddoes [4] suggested using n=2 and c_1=1.359, c_2=-0.359, b_1=-1 and b_2=-4. Wang and Coton suggested adjusting the Φ–function in an effort to approximate the decay rate more accurately. The approach presented uses a different approach. Based on a simplex algorithm a series of "n" linear equations which are solved using a simple LU factorization the analytical Equation (2) is approximated. For each combination of h/r, the optimization algorithm has to determine the following; how many exponential terms are needed and the numerical values for the coefficients c_k, b_k

$$\left.\frac{dw}{dw_0}\right|_{\Omega=\Omega_m} = \frac{|h|\frac{h}{r^2}\left(1-\left(1-\frac{h}{r}\right)cos(\Omega_m)\right)}{\left[1+\left(1-\frac{h}{r}\right)^2-2\left(1-\frac{h}{r}\right)\cos(\Omega_m)\right]^{3/2}} = \sum_{k=1}^{n} c_k e^{b_k\frac{\Omega_m}{\Phi}} \tag{16}$$

The choice of Ω_m is subjected to a weighting function which gives extra significance to values near the bound vorticity.

$$\Omega_m = \frac{2(m-1)}{\pi}\left[1-0.9\left(1-\frac{(m-1)}{(n-1)}\right)^3\right] \tag{17}$$

where m ∈ [1..n] and should implemented as an integer value. The simplex gradient method operates on the principal coming up with b_k coefficients. The initial condition for the gradient method is taken from Beddoes first approximation. The c_k coefficients are found solving the linear set of equations

$$\begin{bmatrix} c_1 e^{b_1 \frac{\Omega_1}{\Phi}} & c_2 e^{b_2 \frac{\Omega_1}{\Phi}} & c_3 e^{b_3 \frac{\Omega_1}{\Phi}} & \cdots & c_n e^{b_n \frac{\Omega_1}{\Phi}} \\ c_1 e^{b_1 \frac{\Omega_2}{\Phi}} & c_2 e^{b_2 \frac{\Omega_2}{\Phi}} & c_3 e^{b_3 \frac{\Omega_2}{\Phi}} & & c_n e^{b_n \frac{\Omega_2}{\Phi}} \\ & \vdots & & \ddots & \vdots \\ c_1 e^{b_1 \frac{\Omega_m}{\Phi}} & c_2 e^{b_2 \frac{\Omega_m}{\Phi}} & c_3 e^{b_3 \frac{\Omega_m}{\Phi}} & \cdots & c_n e^{b_n \frac{\Omega_m}{\Phi}} \end{bmatrix} \begin{bmatrix} dw/dw_0|_{\Omega=\Omega_1} \\ dw/dw_0|_{\Omega=\Omega_2} \\ \vdots \\ dw/dw_0|_{\Omega=\Omega_m} \end{bmatrix} \quad (18)$$

, which after a simple LU factorization yields the c_k coefficients. Based on an arbitrarily selected h/r equal to minus 0.275 and n=6 and n=9 the found coefficients have been tabularized in Table A.1. The influence of the analytical solution of Equation (2) by comparison with the approximation in Equation (7) using coefficients specified in A.1 (n=6) is illustrated in Figure 3. A near perfect approximation to Equation (2) is obtained using the six coefficients for vortex filaments lying throughout the full range. However, a modification of Equation (10) was made as specified by Madsen et al [9], in which Φ avoids becoming zero for 1+h/2r=0. The modification is simply to replace 1+h/2r with a constant value equal to (1-0.25) for all cases where h/2r>0.25 and then let the optimization algorithm approximate the decay rate given by the analytical Equation (2). It should be mentioned that another correction has been given by Wang and Coton [16].

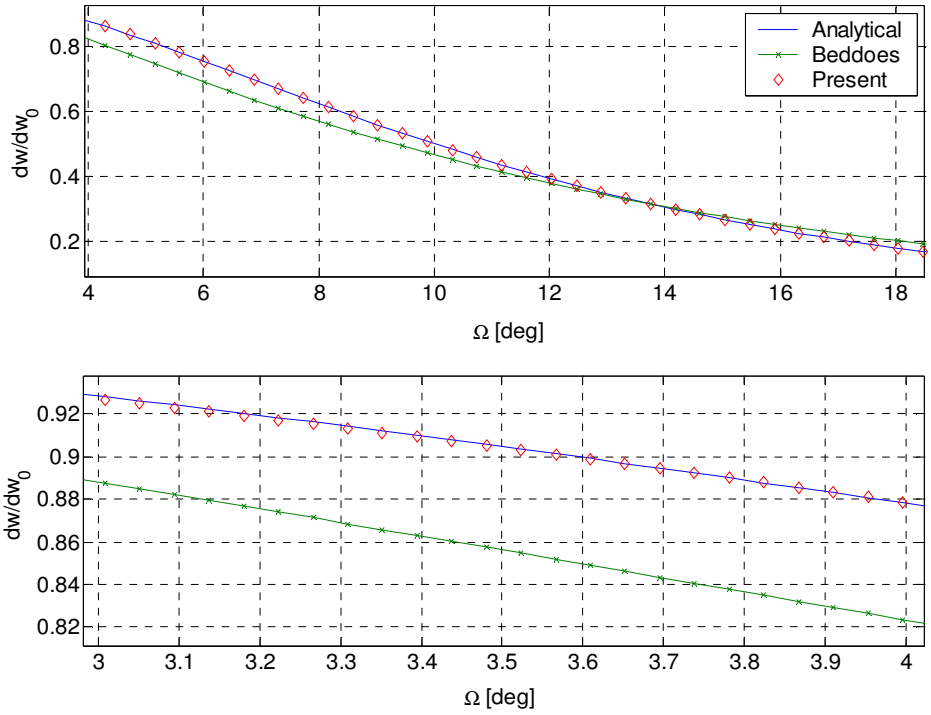

Figure 3; illustrates a comparison of the downwash decay rate for h/r=-0.275 between the analytical solution from Equation (2), Beddoes two term exponential approximation and the presented exponential approximation for n=6.

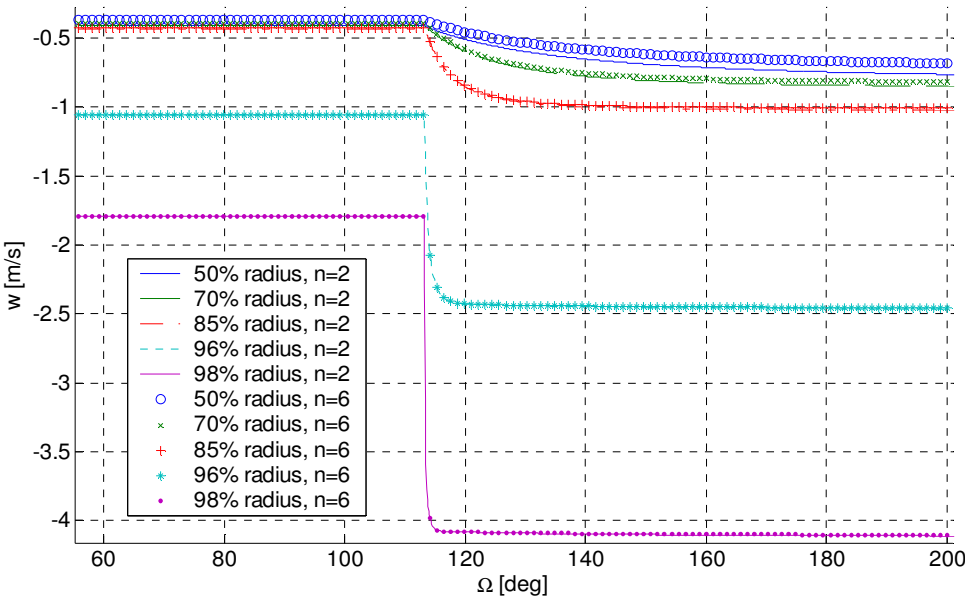

Figure 4; two sets of downwash development at different radial positions for the rotating blade, an equivalent pitch step of -5 degrees at azimuth position 114 degrees is performed. Set one comprise the original Beddoes decay rate and the markers represents the n=6 exponential fit option.

At a given azimuth position a pitch step of -5 degrees is applied. The development of the downwash at different radial positions is shown in Figure 4. An almost immediate response of the downwash is seen at the blade tip, whereas, a mush slower build-up takes place on the middle part of the blade. The figure furthermore illustrates the difference between using near wake decay factors presented by Beddoes (n=2) and a tuned set of exponential coefficients based on n=6. For the fast response in downwash on the outer part of the blade very little difference is seen between the two sets, whereas, a larger difference is seen near the inner part of the blade. The tuned set seems to predict a slower growth in axial induction compared to the original coefficient set, the original Beddoes formulation over predicts the induced velocity when compared with the present formulation using six tuned exponential coefficients.

To speed up the simulation the present model can be extended to include a sub time domain which divides the vortex element at a given time into smaller elements. The state variables used to describe the decay rate follows Equation (9) and (14) with the exception that the delta azimuthal step *"ΔΩ"* has to be divided by the number of substeps *"p"*.

$$Z_k(i) = Z_k(i-1)e^{b_k\frac{\Delta\Omega}{p\Phi}} + c_k\frac{D_w}{p}e^{b_k\frac{\Delta\Omega}{2p\Phi}} \tag{19}$$

The sub time domain has been implemented as specified in Equation (19) in the aero-elastic tool, results from to radial positions are shown in the following figure;

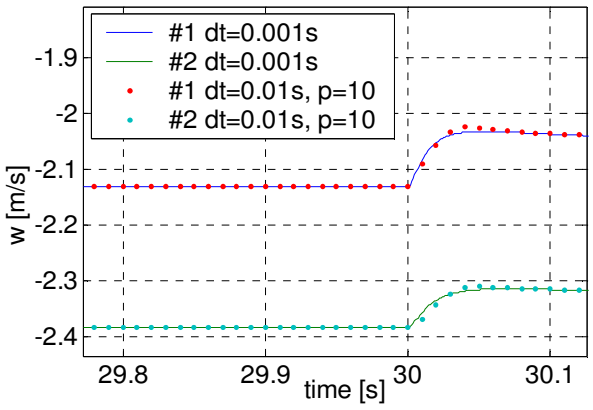

Figure 5; illustrates step changes in axial induction for two radial positions calculated with time steps of 0.001 second and 0.01 second length but with the domain subdivided in 10 equal portions (p=10)

Notice how well a time simulation with time steps of 0.01 seconds compare with the finer time steps of 0.001 second this is due to the sub time domain (p=10) used for 0.01 sound runs.

For the outer ten meter of an imaginary thousand meter long blade a prescribed elliptical bound vorticity was used.

$$\Gamma = \Gamma_{max}\sqrt{1-\left(\frac{r}{r^*}\right)^2} \tag{20}$$

Γ_{max} represents max circulation or elliptic peek value and r^* the half width of the ellipsis which is five meters, r is the free variable runs from 990 to 1000 meter radial wise. Using this long blade offers validity to the two dimensionality assumption and because of the elliptical circulation the induction can be expressed in the analytical form, where a minus sign have been added due to the sign notation in the aero-elastic code used;

$$w = -\Gamma_{max}\frac{1}{4r^*} \tag{21}$$

A comparison of the computed downwash with the analytical downwash, in Figure 6, shows near perfect agreement over the central part and small deviations at the ends *(r=990 and 1000 meters)*.

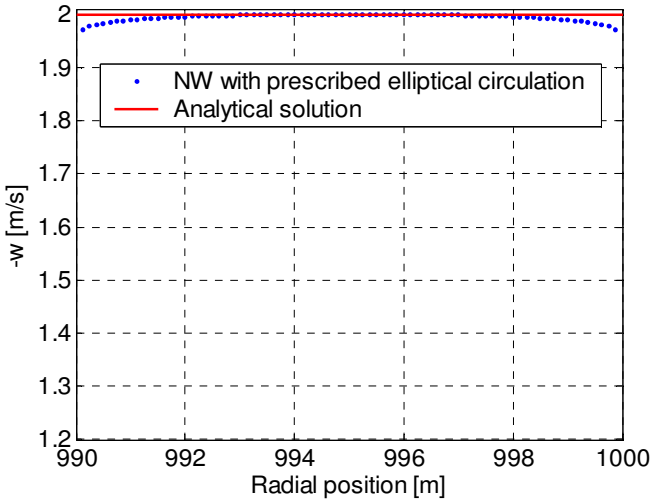

Figure 6; downwash for elliptical circulation

The small deviations near the ends could perhaps be improved using better discretization techniques, but the agreement is deemed acceptable for our purpose of our applications.

FAR WAKE:

In order to calculate the induction field of the rotor, it is important that the amount and direction vorticity trailed and shed into the wake by the blades are represented correctly. The trailed vorticity from the near wake represents one parts of the dynamic wake which handles the instantaneous downwash caused by elastic deformations in the different vibrational modes from tower-dominated modes to blade-dominated modes and in the future possibly the effects of Deformable Trailing Edge Flap (DTEF) devices. The slow variations in the induction, however, like changes in the average wind speed should come from a far wake model. The far wake model by Madsen [9] is used in the present work. The wake integration consists of applying an imaginary scissor which cuts out a 90 degree rotation slice behind each blade and replaces the slice by the near wake model previously described. There is a considerable difference in radial downwash variation for rotating blade when comparing the variation computed with a near wake model and with a BEM model. Along the central part of the blade the near wake predicts a lower induction because the far wake is missing. The far wake model should be adjusted, on the other hand, to compute the induction from the far wake of the blade in question and the wake contribution from the neighbor blades. The dynamic inflow model is baseline for the far wake, the 90 degree rotational wake cut is implemented by applying the far wake load scaling coefficient *(k_{fw})* to the local thrust coefficient for an annular blade element;

$$C_{T,fw} = \frac{V^2 c_N c k_{fw}}{V_\infty^2 2\pi \Delta r} \quad , \tag{22}$$

in which V is the relative wind speed seen by the section, c_N the normal force coefficient, and the annular blade slice is Δr and undisturbed wind speed is V_∞. Through a third order polynomial the steady axial induction factor is determined

$$a = k_1 \left(\frac{C_{T,fw}}{F}\right)^3 + k_2 \left(\frac{C_{T,fw}}{F}\right)^2 + k_3 \frac{C_{T,fw}}{F} + k_4 \quad , \tag{23}$$

where *F* is Prandtl's correction factor, which is unity because the near wake captures the effect of the tip vortex, and the constants k_1 to k_4 are rooted in one dimensional momentum theory. The steady induction can be corrected for yawed and tilted flow misalignments, after which the unsteady induction is added using the indicial function technique adding an element of the dynamic inflow to the model, which in discrete form is

$$z_n^{k+1} = z_n^k e^{-\frac{dt}{\tau_n}} + A_n a \left(1 - e^{-\frac{dt}{\tau_n}}\right) \quad , \tag{24}$$

where *z* is the wake state variables, t_n the time constants and A_n the mixing coefficients for the indicial functions. The time constants have been normalized and approximated in the work of Sørensen *et at.* [12] and shown radial dependency which can be approximated be a second order polynomial with k_n constant coefficients and blade radius *R*

$$\tau_n(r) = k_{n,2} \left(\frac{r}{R}\right)^2 + k_{n,1} \left(\frac{r}{R}\right) + k_{n,0} \tag{25}$$

After adding the present Near Wake model in the aero-elastic code the dynamic inflow model needs re-tuning, this has been done in the work of Andersen *et al.* [3].

A parameter study was performed in which the scaling factor *(k_{fw})* was determined for a variety of tip speeds and rotor thrusts. By scaling the far wake and adding the near wake model and comparing with a BEM model using Prandtl's tip-loss correction [6] it was possible to find k_{fw} using a simple iterative process for a number of λ, C_T combinations. No attempt was made to redesigning the planform in order to maintain the shape of the bound vorticity while varying the tip speeds and pitch settings. The shape of the bound vorticity will change as will the magnitude of the circulation during an increase in pitch angle, consequently the general validity of the investigation for all planforms may be compromised, in an afford to counteract this several planforms have been used in the investigation. The objective function used by this iterative process follows the equation;

$$\int_0^R w_{BEM}\, dr = \int_0^R w_{BEM}(\mathrm{k_{fw}}) dr + \int_0^R w_{NW} dr \tag{26}$$

The parameter study was first performed using the planform given in Appendix A, the result is shown in Figure 7 (top), notice how the value is close to 2.7 suggested by Madsen [9]. Another planform was investigated; the result of using the commercial planform is shown in Figure 7 (bottom). Although the two planforms, profile data and control strategy are different the k_{fw} dependency of λ, C_T appears similar, which gives enough confidence to proceed by performing a 3D least square fit to the $k_{fw}(\lambda,C_T)$ surface. The following equation for the surface was chosen

$$k_{fw}(\lambda, C_T) = l_1\lambda^4 + l_2\lambda^3 + l_3\lambda^2 + l_4\lambda + l_5{C_T}^4 + l_6{C_T}^3 + l_7{C_T}^2 + l_8C_T + l_9\lambda C_T + l_{10} \tag{27}$$

$$\begin{bmatrix} l_1 \\ \vdots \\ l_n \end{bmatrix} = \begin{bmatrix} \lambda_1^4 & \lambda_1^3 & \lambda_1^2 & \lambda_1 & {C_T}_1^4 & {C_T}_1^3 & {C_T}_1^2 & C_{T_1} & \lambda_1 C_{T_1} & 1 \\ \vdots & \vdots & \vdots & \vdots & \vdots & \vdots & \vdots & \vdots & \vdots & \vdots \\ \lambda_o^4 & \lambda_o^3 & \lambda_o^2 & \lambda_o & {C_T}_o^4 & {C_T}_o^3 & {C_T}_o^2 & C_{T_o} & \lambda_o C_{T_o} & 1 \end{bmatrix} / \begin{bmatrix} k_{fw}(\lambda_1, C_{T_1}) \\ \vdots \\ k_{fw}(\lambda_o, C_{T_o}) \end{bmatrix} \tag{28}$$

, in which "$l_{1..n}$" are constants to be determined using the following least square fitting method based on LU decomposition by backwards and forward substitution indicated as "/" and index "o" is the number of simulations run 110 was used $10\lambda \cdot 11C_T$. Solving this equation gives the following coefficients for the fitted surface

$$l_n=[-9.02\cdot10^4 \;\; 0.0241 \;\; -0.213 \;\; 0.676 \;\; -2.35 \;\; 5.97 \;\; -4.95 \;\; 1.30 \;\; 0.0257 \;\; 2.20]^T.$$

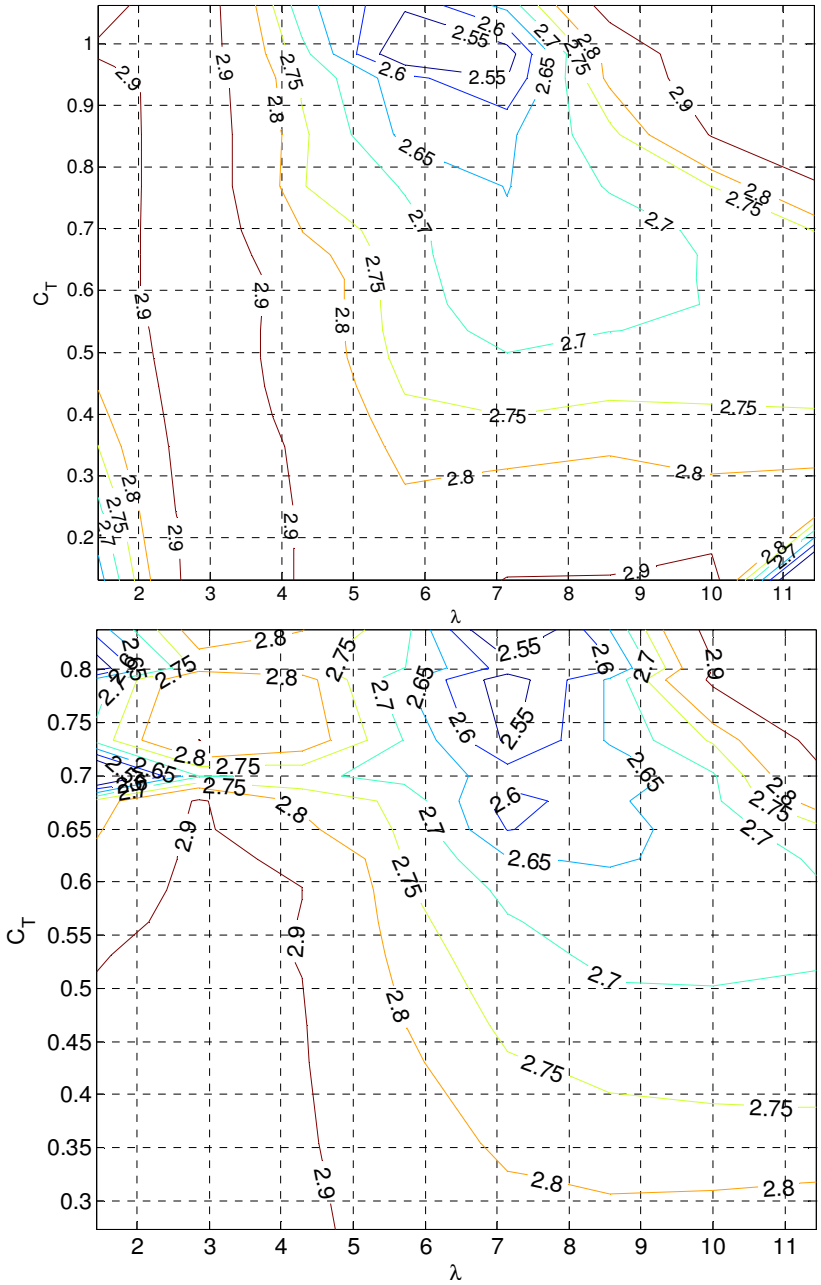

Figure 7; the far wake load calibration (k_{fw}) coefficient is plotted for different rotor loadings (C_T) and tip-speed ratios (λ). The variation in thrust stems from changing the pitch; whereas, λ is changed by a varying the rotational speed. The bound circulation is not kept constant but can changes for each $k_{fw}(\lambda,C_T)$ point. (TOP) The imaginary rotor uses 40 meter blades for which the planform is specified in appendix A, profile data follows $C_L=2\pi\alpha$, $C_D=C_M=0$. (BOTTOM) shows a similar study using a commercial rotor as baseline.

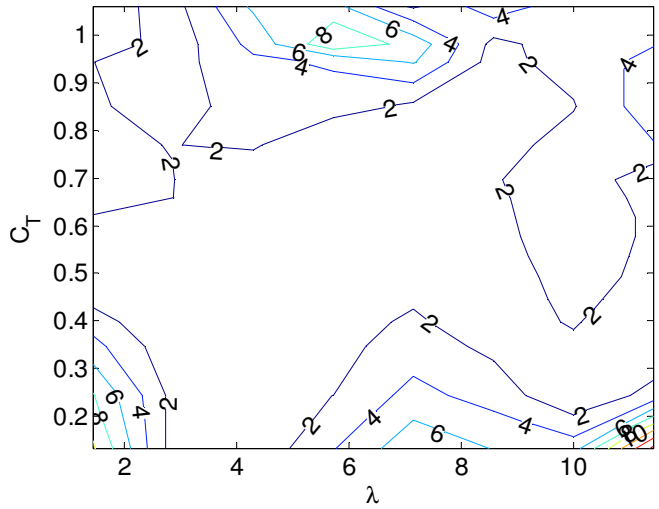

Figure 8; percent error between the fitted far wake calibration surface and the far wake calibration coefficients $k_{fw}(\lambda,C_T)$.

The percent error between the fitted surface and the actual far wake load calibration coefficients is shown in Figure 8, for the normal operation ranges the error is within two percent. The optimal tip-speed is 8 and the thrust coefficient is 8/9 for the rotor described in Appendix A. In general a variable speed with patchable blades operating in the power control region the thrust coefficient drops as the blades starts pitching, furthermore the tip-speed should be expected to also drop after the constant rotational speed is reached.

SHED VORTICITY:

Only the downwash from the trailed vorticity system has been considered, the other important part of the dynamic downwash includes the shed vorticity. The trailed vorticity is related to $\delta\Gamma/\delta r$ and the shed vorticity is related to $\delta\Gamma/\delta V\, dt$, V being the wind relative to a blade section. The analytical solution for the two dimensional shed vorticity problem was derived by Theodorsen [14] an efficient numerical algorithm can be derived using an indicial function representation of the effective angle of attack [8]. This work was further extended to include a deformable trailing edge flap which is modeled by a series of modal expanded camberline shapes in the work of Gaunaa [5]. Finally the modal expanded camberline code was merged with the Beddoes-Leishman type dynamic stall model by Andersen et al. [2].

RESULT AND DISCUSSION:

The present Near Wake (NW) model is compared with the original Blade Element Momentum (BEM) model. The Far Wake (FW) contribution to the downwash using the FW calibration coefficient is included in the comparison. The radial variation of the downwash distribution for the rotating blade computed with the components of the NW model, the scaled FW BEM model the pure BEM model is shown in Figure 9.

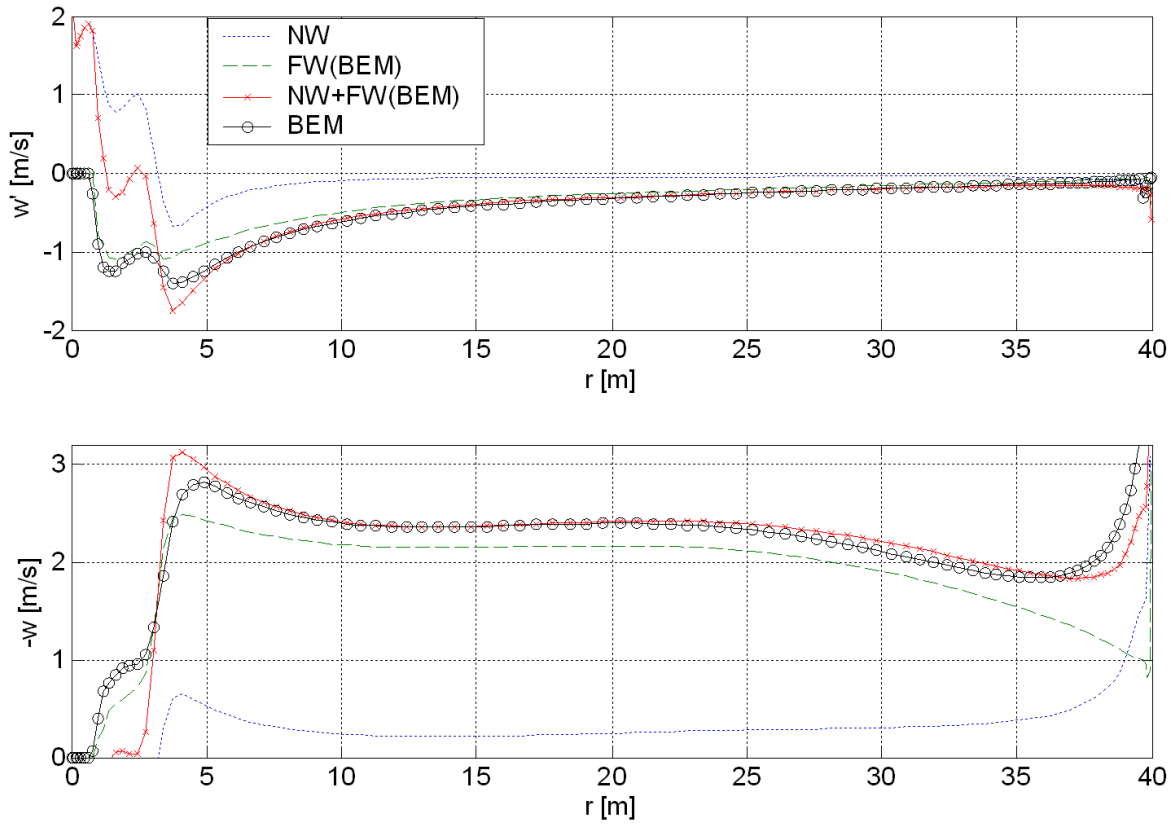

Figure 9; induction from the Near Wake (NW), the Far Wake (FW) and the combined NW+FW compared to the wake using a BEM code with the traditional tip correction. (top) tangential induction along the blade for present and the BEM model. (bottom) axial induction along the blade.

Calculations performed using the planform specified in Appendix B, constant direct inflow conditions at 7m/s, rotational speed of rotor 1.70 rad/s. Wang and Coton's [16] cross-plane convection is applied. Notably the present model also models the effects of the tip vortex. Some difference exists locally between the BEM model and the present model with regard to the axial induction for the outer and inner part of the blade; however, on the integral blade scale the steady state induction is identical.

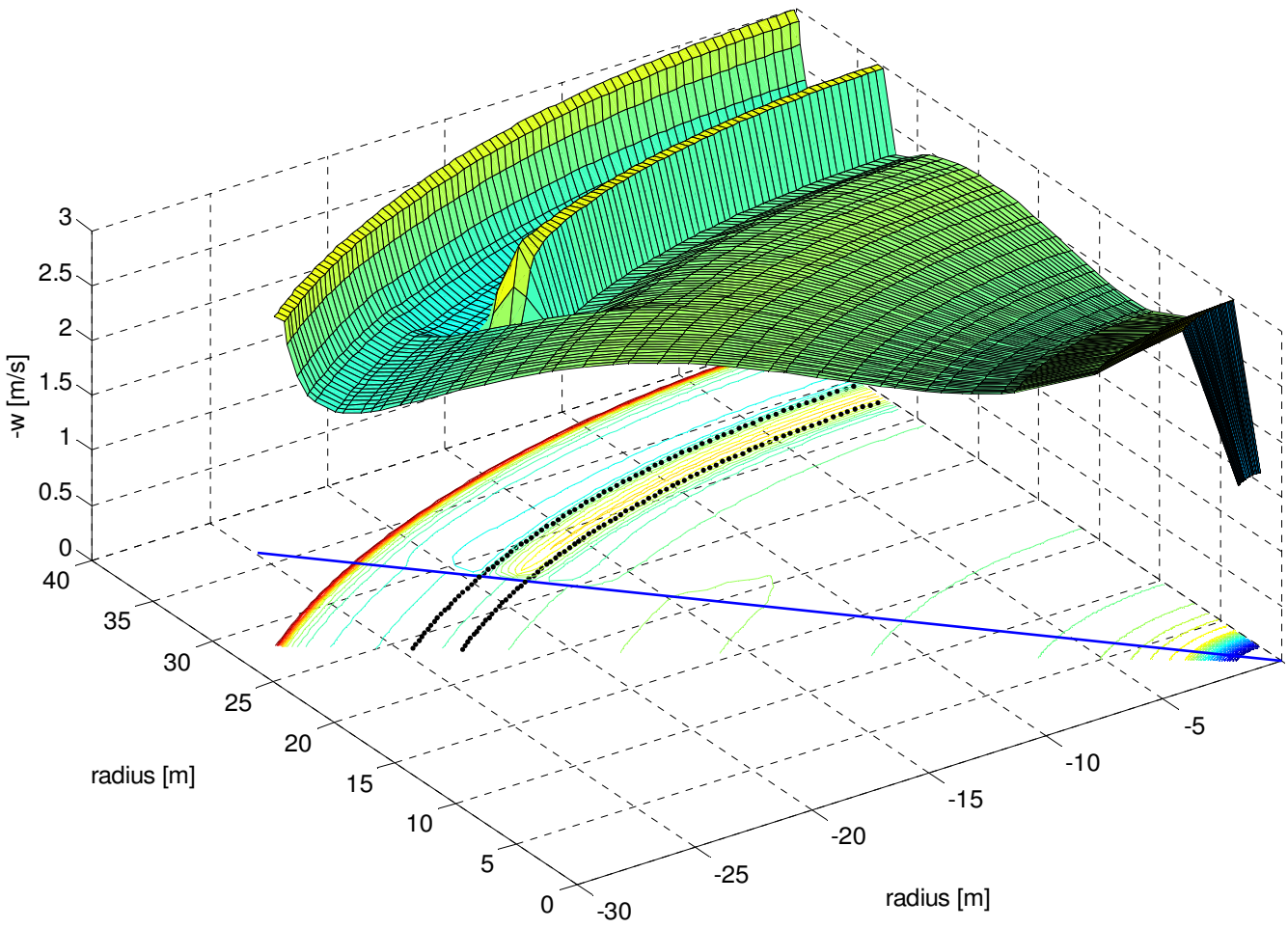

Figure 10; illustrates snap shots of the rotated axial downwash for given constant time intervals. A two meter Deformable Trailing Edge Flap (DTEF) is mounted on the blade at radius 32 to 34 meter. The DTEF is actuating three degree downwards in a step change. The location of the DTEF is illustrated by the concentric dotted balls, and the time of actuation is shown by the strait line crossing origo. The DTEF is part of a Beddoes-Leishman type dynamic stall model; this model also includes the effect of shed vorticity and an unsteady modal expanded camberline formulation [2].

The time development of the downwash is illustrated in Figure 10 as a combined contour surface plot. The strong downwash at the tip as well as at the blade root is the most recognizable feature. One of the main advantages of the present model in comparison with BEM theory is that the downwash at a point on the blade is influenced by the trailed vorticity from all the other points on the blade. This means that changes in the aerodynamic properties locally on the blade will have some influences on the downwash at the neighboring sections. Examples of local changes are the use of DTEF's or sometimes referred to as flapping devises, stall strips and vortex generators. The effect of a DTEF is illustrated here on the blade where a two meter long DTEF is mounted on the outer part of the blade. In Figure 10 a three degree step change in flap angle causes a resulting development in induction for a much larger part of the blade than the two meter which originated the change.

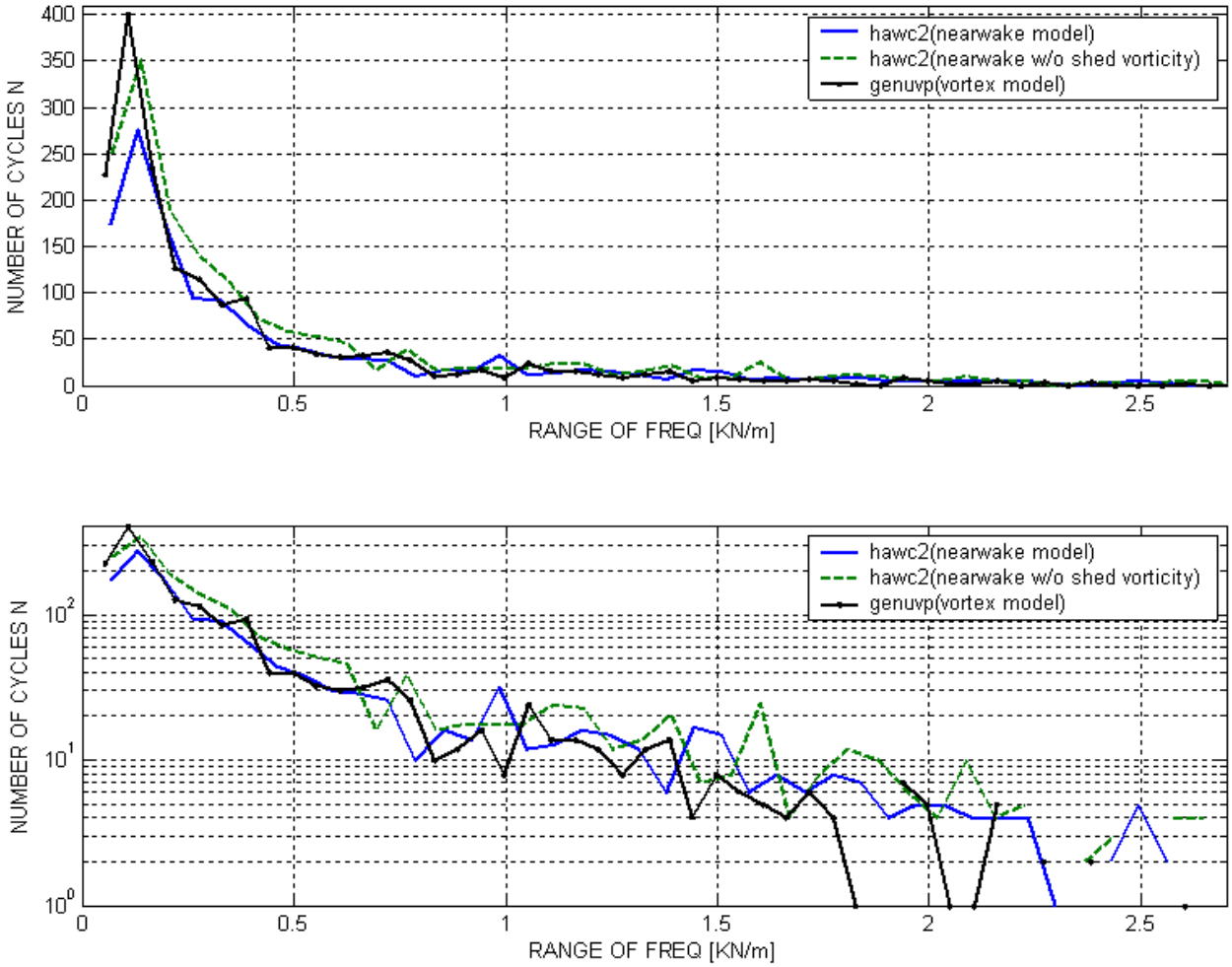

Figure 11; comparison between HAWC2 with and without shed vorticity and the GENUVP from CRES using the rainflow counting technique.

The 5 Mega Watt reference turbine used in the UpWind project [13], running at constant rotor rotational speed at 8m/s mean turbulent wind using 15% turbulence intensity have been used to make comparisons between the GENeral Unsteady Vortex Particle (GENUVP) code [15] developed at the National Technical University of Athens (NTUA) and the present Near Wake model. The comparisons was carried out using the rainflow counting technique in which normal force amplitudes at 75% radius for a ten minute simulated series was counted, the result is shown in Figure 11. There is a good agreement between the two models for most regions of amplitudes counted; however, there is a discrepancy in small amplitudes. GENUVP predicts nearly 60% more small oscillations than the present Near Wake model. An initial parameter investigation in which the shed vorticity and the circulation lag were disabled did not provide the necessary increase in the quantity of small vibrations for the present model. Further investigations are needed, it has been suggested that the discrepancy between the two models may lie in the interpolation procedure for the turbulence box.

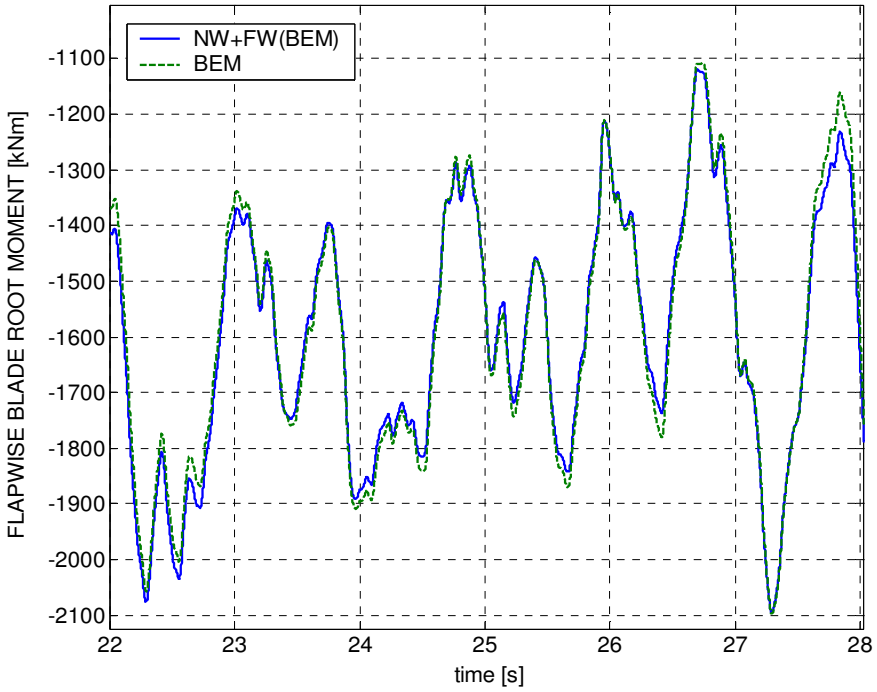

Figure 12; illustrates the flapwise blade root moment for the two cases using the 80 meter diameter rotor from Appendix A.

A comparison between the traditional BEM model and the present NW model is shown in Figure 12 using the simulated flapwise blade root bending moment as sensor output. Despite the discrepancy in induction locally between BEM and the present NW model, the integral dynamics represented by the root bending moment appears close to identical. Further investigation could suggest the origin of the difference to be due to inaccurately tuned time constants still active in the FW dynamic inflow part used in the present model. Currently the inflow time constants remain unaltered from the dynamic inflow model used in the traditional BEM model.

CONCLUSION:

A Near Wake (NW) model has been implemented in the aero-elastic tool HAWC2 [7] developed at the Danish National Laboratory for Renewable Energy Risø/DTU. The NW model clearly captures the same inductional tip effects as Prandtl for the Blade Element Momentum (BEM) model. A series of Deformable Trailing Edge Flaps (DTEF) has been mounted on the five mega watt reference turbine used in the UpWind project [13]. By activating the DTEF's the induction clearly shows tendencies to couple in the radial direction, which is not the case for the BEM formulation, where the induction only couple through the elastic beam elements. The calculated induction from the elliptic circulation near the tip of a very large blade (1000m) is close to the analytical induction when using the NW model.

The present model is compared to the GENeral Unsteady Vortex Particle (GENUVP) model [15] developed at the National Technical University of Athens. The normal force at 75% radius is compared using the rainflow counting technique. The result of this comparison shows a strong correlation between GENUVP and HAWC2 for

most frequencies, however, it may be prudent to conduct further investigation into the high-frequency discrepancies the differences may be due to how the turbulence is read and wind components are interpolated along the blade.

In the work of Madsen [9] an investigation of aerodynamic work by sinusoidal fluctuation in the NW was carried out, this and an investigation into aerodynamic damping still remains to be carried out.

Further investigation is needed with regard to the general validity of using a single far wake scaling factor surface for all blades.

REFERENCES:

[1] Andersen, P.B.; Gaunaa, M.; Bak, C.; Buhl, T., Henriksen L.C., "Integrating Deformable Trailing Edge Geometry in Modern Mega-Watt Wind Turbine Controllers" In: Proceedings (online). 2008 European Wind Energy Conference and Exhibition, Brussels, 29 Mar -4 Apr 2008. (European Wind Energy Association, Brussels, 2008) 14 p

[2] Andersen P.B., Gaunaa M., Bak C., M.H., "A Dynamic Stall Model for Airfoils with Deformable Trailing Edges" Journal of Physics 5, 2007. 14p

[3] Andersen, P.A., Madsen, H.Aa, Sørensen, N.N., "Implementing Dynamic Inflow using Indicial Function Formulation in a Multi Body Aero-Elastic Code" (to appear)

[4] Beddoes T.S., "A near wake dynamic model." Aerodynamics and Aeroacoustics National Specialist Meeting. Papers and Discussion, 1987; 1-9

[5] Gaunaa, M. "Unsteady 2D Potential –flow Forces on a Thin Variable Geometry Airfoil Undergoing Arbitrary Motion", Risø-R-1478, Risø, Roskilde, Denmark, June 2004.

[6] Hansen, M. "Basic Rotor Aerodynamics applied to Wind Turbines", ET-NE 98-02, ISBN: 87-7475-192-1, Department of Mechanical Engineering, Technical University of Denmark.

[7] Larsen, T.J.; Hansen, A.M., How 2 HAWC2, the user's manual. Risø-R-1597(ver. 3-1)(EN) (2007) 70 p.

[8] Leishman JG. "Principles of Helecopter Aerodynamics". Cambridge University Press: Cambridge 2000.

[9] Madsen H.Aa, Rasmussen F., "A Near Wake Model for Trailing Vorticity Compared with the Blade Element Momentum Theory". Wind Energy Article 2004; 7; 325-341

[10] Schepers JG, Snel H., "Dynamic inflow: yawed conditions and partial span pitch control", ECN-C—95-056, 1995.

[11] Snel H., "Survey of induction dynamics modeling within BEM-like codes", AIAA Paper 2001-0027, 2001.

[12] Sørensen, N.N.; Aagaard Madsen, H., “Modelling of transient wind turbine loads during pitch motion” (paper and poster). In: Proceedings (online). 2006 European Wind Energy Conference and Exhibition, Athens (GR), 27 Feb - 2 Mar 2006. (European Wind Energy Association, Brussels, 2006) 10 p

[13] Sørensen, N.N.; Johansen, J., “UpWind, aerodynamics and aero-elasticity, rotor aerodynamics in atmospheric shear flow” (Invited Paper and Presentation). In: Conference proceedings (online). 2007 European Wind Energy Conference and Exhibition, Milan (IT), 7-10 May 2007. (EWEA, Brussels, 2007) 9 p.

[14] Theodorsen T. “General theory of aerodynamic instability and the mechanism of flutter”. NACA Report 496, 1935.

[15] Voutsinas, S.G., “A generalized unsteady vortex particle method for solving the unsteady flow around multi-component configurations. “,1990. NTUA Internal Report, National Technical University of Athens, Athens, Greece.

[16] Wang T, Coton FN. “A modified near wake dynamic model for rotor analysis”. The Aeronautical Journal 1999; 103: 143-146.

APPENDIX A:

		k=1	2	3	4	5	6	7	8	9	$\Sigma\varepsilon^2$
(A)	c_k	1.3590	-0.3590								0.136
	b_k	-1.0000	-4.0000								
(B)	c_k	5.4531	2.7266	1.3633	0.6816	0.3408	0.1704				$2.7e^{-7}$
	b_k	0.0594	-1.4211	2.2969	-0.0404	0.2367	-0.1314				
(C)	c_k	5.7500	2.8750	1.4375	0.7187	0.3594	0.1797	0.0898	0.0449	0.0225	$2.0e^{-7}$
	b_k	0.3997	-2.0504	2.8331	-1.3071	5.0194	-15.904	35.751	-42.887	19.145	

Table A.1 (A) coefficients from Beddoes two term exponential approximations, (B) presented six term exponential approximations and (C) nine term approximation. Summed squared residual to the analytical solution is presented in the last column for comparison. It should be noted that the tuned coefficients in (B) and (C) are specifically for h/r=-0.275.

Radius [m]	Chord [m]	Twist [deg]
0.0000	4.0000	15.0000
4.0000	3.7000	10.9350
8.0000	3.4000	7.6800
12.0000	3.1000	5.1450
16.0000	2.8000	3.2400
20.0000	2.5000	1.8750
24.0000	2.2000	0.9600
28.0000	1.9000	0.4050
32.0000	1.6000	0.1200
36.0000	1.3000	0.0150
38.6667	1.1000	0.0019
40.0000	1.0000	0.0002

Table A.1; planform data for the 40m blade, all profiles assumed to have $2\pi\alpha$ lift coefficient with zero drag and moment coefficients.